Microstructure characterization of amorphous thin solid films in a fringe-free environment

Tong Li and Jerzy Kanicki[a)]
Center for Display Technology and Manufacturing, Department of Electrical Engineering and Computer Science, The University of Michigan, 3300 Plymouth Road, Ann Arbor, Michigan 48105

(Received 21 July 1998; accepted for publication 22 September 1998)

We have comprehensively analyzed the influence of the probe beam's polarization state and incident angle on the vibrational absorption spectra of thin solid films such as hydrogenated amorphous silicon nitride and hydrogenated amorphous silicon in Fourier transform infrared spectroscopy. This analysis demonstrates the nuisance of interference fringes in distorting the bond structure of thin solid films in conventional vibrational absorption spectra. Based on the spectrum analysis and optical fundamentals, a practical method of recording a vibrational absorption spectrum of a thin solid film in an interference fringe-free environment is proposed. Furthermore, it is also demonstrated that a fringe-free spectrum can be recorded even in an interference-embedded environment if a right light incident angle is chosen. This interference-embedded fringe-free spectrum is only valid for material's qualitative microstructure assessment but not for direct quantitative analysis. Finally, a comparison between ideal spectra and those fringe-corrected by conventional measures indicates a nontrivial discrepancy. Therefore, only interference-free spectrum exhibits the absolute features of the bond structures, and should be the standard spectrum used for thin solid film microstructure assessment. © *1999 American Institute of Physics.* [S0021-8979(99)00401-6]

I. INTRODUCTION

Amorphous thin films such as hydrogenated amorphous silicon (*a*-Si:H), hydrogenated amorphous silicon nitride (a-SiN_x:H) and amorphous silicon oxide (a-SiO_x) deposited by plasma-enhanced chemical vapor deposition (PECVD) are critical materials in the application of amorphous silicon thin-film transistors (*a*-Si:H TFTs). They must fulfill stringent electrical requirements which are strongly influenced by the film's microstructure such as hydrogen (H) content, di- and mono-hydro species ratio, stoichiometry, etc.[1,2] The characterization of this microstructure is normally represented by the film's vibrational absorption spectra obtained using a technique called Fourier transform infrared spectroscopy (FTIR),[3,4] in which thin films are normally deposited on double side polished Si wafers and are then scanned with their surfaces normal to probe beam. Vibrational absorption spectrum recorded in this way usually contains fringes due to constructive and destructive interference of the beams resulting from partial reflection at the film's interfaces. The features of peak density (shapes) in the fringe-embedded spectrum are not only distorted by the fringes, but also amplified and/or deviated by the partial reflection.[5–7] Therefore, correction is needed either during or after scanning. Conventionally, efforts to remove or minimize fringes are made in three practical ways: subtract a mathematically generated fringe pattern (which matches the spectrum baseline) from the measured spectrum,[8] use a wedged double side polished Si wafer as a substrate,[9] and deposit a very thin layer of film ($\sim$100 nm) (such that fringes' spacing is so large that the interested range of the spectrum baseline is almost straight).[10] These measures do reduce fringe effect to some extent, however, none of them can remove fringes completely and reliably. Furthermore, correction of density amplification seems impossible in this fringe-embedded spectrum. However, this kind of distorted vibrational absorption spectra has been widely used in the past,[11,12] and many important properties such as H content, stoichiometry, etc. were derived from them using parameters calibrated with respect to this conventional spectra.[13–16] Unfortunately, the applicability of these conventional parameters is very limited. For example, bond absorption strength coefficients of a-SiN_x:H derived conventionally have a large variation, which could be as large as 50%.[16] As a matter of fact, conventional bond absorption strength coefficients are only valid for the films from which these coefficients are calibrated, and are invalid for films with different H content or stoichiometry. Since the film's refractive index, which determines the reflectance at film's interface, varies with stoichiometry, H content and doping level, different films will have different effective absorption strength.[17]

To remove interference fringes and density amplification from the spectrum, apparently it is essential to avoid or minimize the partial reflection at the film's interfaces. In this article, we analyze the probe beam's polarization state and incident angle influence on the vibrational absorption spectra of a-SiN_x:H and *a*-Si:H thin films. Based on this analysis and optical fundamentals, we propose a method of collecting vibrational absorption spectrum free of interference fringes by utilizing the Brewster law (a concept not fresh in spectroscopy in general[18] but not yet applied in this specific area somehow). Furthermore, we also demonstrate that a fringe-

a)Electronic mail: kanicki@eecs.umich.edu

TABLE I. Film deposition conditions and fundamental parameters used in this study. The refractive index was measured in the spectral range between 2000 and 2500 cm^{-1}.

	NH_3 (sccm)	SiH_4 (sccm)	Pressure (Torr)	T_{sub} (°C)	Thickness (nm)	n
a-SiN_x:H	200	18	0.43	250	100	1.88
a-Si:H	—	50	0.43	250	900	3.27

free but not an interference-free spectrum can be realized even with an unpolarized light source. Finally, a comparison between conventionally baseline corrected and ideal spectra is given to illustrate a nontrivial distortion of conventionally fringe-corrected spectrum in terms of portraying the material's microstructure.

II. EXPERIMENT

The a-SiN_x:H and a-Si:H thin films were deposited on double side polished Si wafers in PECVD system using standard rf excitation at substrate temperature of 250 °C. The films' thickness is then measured using a Dektak profiler. Details of the films' deposition condition and fundamental properties used in this study are tabulated in Table I. It must be pointed out that a-Si:H thin film used in this study was intentionally grown with a high concentration of SiH_2 bond to illustrate the difference between various baseline corrections and fringe-free spectra.

The film's refractive index is deduced from infrared (IR) spectrum by observing a straight baseline at Brewster angle using p-polarized light (see Sec. I). Likewise, the Si wafer's refractive index is deduced by observing maximum gain using the IR spectrometer at Brewster angle with p-polarized light, because full energy transmission can be realized at this point. The Si wafer is assumed to be nonabsorbing, since no significant absorption overlaps the absorption peak of the thin films in the interested spectral region. For the absorption peaks of the films, although the extinction coefficients exist, most of them are small,[17] and will not cause significant fringe pattern deviation from nonabsorbing baselines. However, for prominent peaks such as 880 cm^{-1} of a-SiN_x:H and 630 cm^{-1} of a-Si:H, the extinction coefficients are nontrivial and will cause significant fringe pattern deviation from the baselines at incident angles other than Brewster.[6,17] When the incident angle approaches Brewster, this deviation becomes insignificant, which is reflected by the fact that at Brewster angle all absorption peaks have minimum densities (see Sec. I). Therefore, for simplicity, the extinction coefficients are ignored in the calculation. Instead, the effective indices obtained from the IR spectrum are used, and hereafter labeled as the refractive indices.

The IR spectra were recorded at room temperature using BioRad FTS-40 FTIR spectrometer and analyzed using BioRad Win-IR software. The spectrum, having a spectral resolution of 8 cm^{-1}, is the average of 64 scans. The aperture of the probe beam was set at 2 cm^{-1} and the detector gain amplification was set at unity.

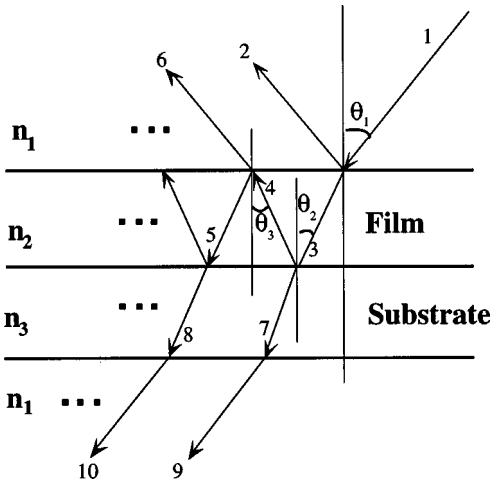

FIG. 1. Illustration of the probe beam passing through the stack of thin film and substrate.

III. OPERATION PRINCIPLE

A. Optical fundamentals

To understand the operation principle, it is necessary to briefly review the fundamentals of interference theory first. Figure 1 illustrates the situation of a thin layer of film on top of the transmissive substrate. As illustrated, when an impinging probe beam (1) strikes the first interface composed of media n_1 and n_2, part of beam (1) is reflected and assigned as beam (2) and the other part is refracted and assigned as beam (3). Beam (3) further undergoes reflection and refraction and splits into beams (4) and (7) at the second interface of n_2 and n_3. The reflection and refraction have been repeated whenever the beam strikes the interfaces. Fringes in the spectra are caused by the constructive and destructive interference of the multicomponents of the beams such as (9), (10), etc. generated from partial reflection of the first and second interfaces of the film. The fringe patterns strongly depend on the beam's optical path which is determined by the film's refractive index, thickness and beam incident angle.[19] It should be noted that the partial reflection from two surfaces within substrate is ignored in the figure, since the Si wafer is usually very thick (>400 μm) which is out of the spatial coherence range, and will not cause fringes in the range of interest. Obviously, if reflected beams (4) or (5) can be eliminated then no beam other than (9) will go through the stack and be collected by the detector in the system. Consequently, no fringes will be observed in the vibrational absorption spectra.

From classic optics we know that an unpolarized beam can be represented by two orthogonal linearly polarized waves of equal amplitude. The one with the vibration plane in the incident plane is identified as parallel E field (p vector), and the one with the E field orthogonal to the incident plane is defined as perpendicular light (s vector). The reflectances of parallel and perpendicular fields at the interface of two media can be described by the following formulas derived from Fresnel equations:[19]

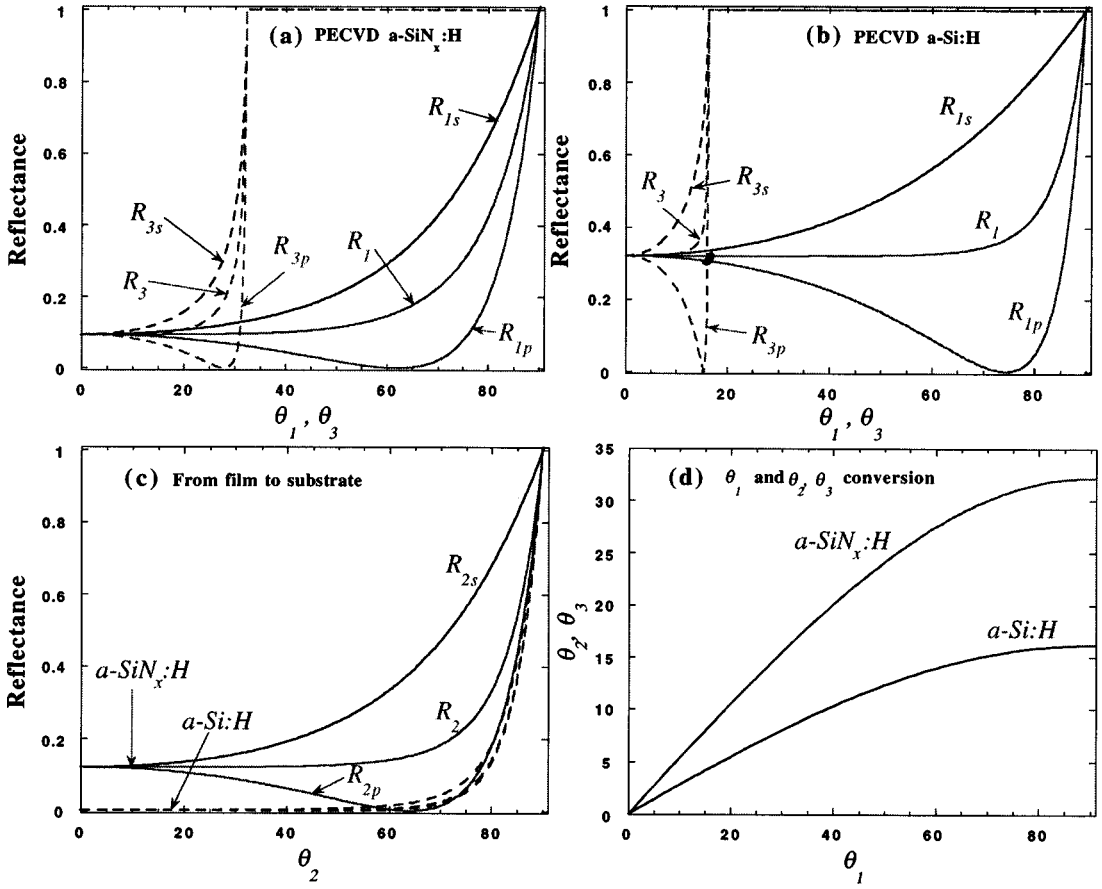

FIG. 2. Parallel (p) and perpendicular (s) polarized light and energy reflectance as a function of incident and refracted angles plotted according to Eq. (1) for different interfaces, where first, second, and third interfaces are represented by film/air, substrate/film, and air/film, respectively. Reflectances of first and third interfaces are illustrated in (a) and (b) for a-SiN$_x$:H, and a-Si:H, respectively. Reflectances of second interfaces are presented in (c) for both a-SiN$_x$:H, and a-Si:H, and the external incident and internal refracted angles' conversion is provided in (d) for direct comparison. The refractive indices used in calculation are 1.88, 3.27, and 3.87 for a-SiN$_x$:H, a-Si:H and Si substrate, respectively.

$$R_p=\frac{\tan^2(\theta_i-\theta_r)}{\tan^2(\theta_i+\theta_r)},$$

$$R_s=\frac{\sin^2(\theta_i-\theta_r)}{\sin^2(\theta_i+\theta_r)}, \tag{1}$$

where θ_i and θ_r represent incident and refracted angles, respectively. From Eq. (1), it is clear that R_s can never be zero, while R_p is zero when the denominator is infinite; that is when $\theta_i+\theta_r=90°$. The total reflection derived from energy conservation is then

$$R=\frac{R_p+R_s}{2}. \tag{2}$$

Since the beam will undergo many reflections at different interfaces and the ratio of the p and s components changes after each reflection and refraction, it is necessary to track the energy flow inside the film. By following energy conservation law, we can derive the energy reflectance (total) at each interface. If we assign the subscript (m) of reflectances according to the order that the light beam strikes the interfaces, namely, R_1, R_2, and R_3 for the reflectances at interfaces composed by media of n_2/n_1, n_3/n_2, and n_1/n_2, respectively, the normalized energies transmitted into film are $1-R_1$, $(1-R_{1s})/2$, $(1-R_{1p})/2$ for total, s- and p- polarized light, respectively. The total reflectance at second interface (film/substrate), following the partial polarization ratio from energy conservation is given as

$$R_2(1-R_1)=R_{2s}\frac{1-R_{1s}}{2}+R_{2p}\frac{1-R_{1p}}{2},$$

$$R_2=\frac{R_{2s}(1-R_{1s})+R_{2p}(1-R_{1p})}{2(1-R_1)}. \tag{3}$$

Likewise, the total reflectance at the third interface (air/film) can be expressed as

$$R_3=\frac{R_{3s}R_{2s}(1-R_{1s})+R_{3p}R_{2p}(1-R_{1p})}{R_{2s}(1-R_{1s})+R_{2p}(1-R_{1p})}, \tag{4}$$

where R_{ms} and R_{mp} ($m=1, 2, 3$) can be calculated using Eq. (1) for corresponding interfaces (media). Curves calculated from Eqs. (1), (2), (3) and (4) are plotted in Figs. 2(a), 2(b) and 2(c) for a-SiN$_x$:H and a-Si:H, respectively, whereas n_1 is taken as unity. These curves serve as guidelines in explaining the observed phenomenon described in the following sections.

The incident angle at which the reflectance for linear polarized light with E parallel to the plane of incident (p)

vanishes and the beam is completely transmitted is called Brewster angle (B angle). This angle can be calculated from

$$\tan \theta_B = \frac{n_r}{n_i}. \tag{5}$$

Equation (5) is derived from the relation of $\theta_i + \theta_r = 90^\circ$ and Snell's law,[15] and is of course the essence of Brewster's law.

When the external incident angle θ_1 is set at B angle, corresponding internal angle θ_3 is also at B angle due to the reversibility of light. This can be easily confirmed by the sum of 90° of θ_{1B} and θ_{3B} in Figs. 2(a) and 2(b). The relation between external and internal angles is plotted using Snell's law in Fig. 2(d) for direct comparison.

B. Optimal angle selection

When a p-polarized probe light impinges the sample, an incident angle has to be selected such that beams (3) or (4) can be completely transmitted at the respective interfaces, that is, no reflected beams (4) or (5) exist. Theoretically, two Brewster angles can be chosen: one is determined by the n_1/n_2 interface and the other is determined by the n_2/n_3 interface. The former makes beam (4) fully transmit into the air while the latter lets beam (3) fully transmit into medium n_3. The application of θ_{1B} is quite straightforward and can be envisioned from Figs. 1 and 2. However θ_{2B} has to be, according to Snell's law, converted to θ_1 at which it is convenient to be set externally. Semiconductor materials usually have a large value of refractive index, therefore the refracted angle is usually small even when the incident angle is very large. For example, the refractive indices of the Si wafer, a-Si:H and a-SiN_x:H in the interested region is 3.87, 3.27 and 1.88, respectively, which yield a θ_{2B} around 42.7°and 62.7° for a-Si:H and a-SiN_x:H, correspondingly. Apparently, these θ_{2B} values are way out of maximum values in Fig. 2(d) and can never be converted to real θ_1 values due to the large value of the film's index ($\sin \theta_1 = n_2 \sin \theta_{2B} > 1$). Even when n_2 is small enough to get a real value of θ_1, this angle is usually so large that the reflectance of the first interface at this angle is very large, and very little energy will be transmitted into the film [Figs. 2(a) and 2(b)]. Therefore it is always convenient to choose the first Brewster angle instead of the second unless the first choice is impossible in some special cases. Since the optimal angle is set at the first interface according to the film's index, the index or nature of the substrate (normally, double side polished Si wafer) only determines the beam path inside the substrate, and has no effect on measurement as long as it satisfies other requirements for IR measurement.

Another relevant incident angle setting is for the background (substrate) scan, since the incident angle determines the path of the beam inside the substrate, and then determines the absorption strength attributed to the substrate. Any inconsistent setting between background and sample scans will result in spectra deviation caused by the improper normalization. The critical issue to keep the consistency is that the refracted angles inside the substrate must be kept constant in both sample and background scans. In the case of sample scan (Fig. 1), the refracted angle inside the substrate, according to Snell's law, is calculated from the product of the film's refractive index and sine of the internal incident angle θ_2 which, in turn, equals the sine of the external incident angle θ_1 (assuming the surrounding medium has an index of unity). Apparently, with or without the thin film layer the refracted angle inside the substrate remains the same as long as the external incident angle θ_1 remains constant.

From the equations in Sec. III A, it is clear that the Brewster condition depends on the refractive index of film. Theoretically, it is impossible to find a Brewster angle for the whole spectrum, since the refractive index varies with the wavelength. Therefore, the proposed method is only applicable to films with a small variation of refractive index within interested spectrum, and/or films with a fairly large thickness (>100 nm) such that the residual interface partial reflection causing fringes is negligible in comparison with the signal (bond absorption densities). Fortunately, in practice, a-Si:H and a-SiN_x:H thin films basically possess the former property while their thickness can always be controlled to compensate for index variation. It is also indicated in Fig. 2 that for films having comparatively small refractive indices the selection to the incident angle has a comparatively larger range, whereas for materials having large refractive indices this freedom is quite limited. In other words, relatively thin a-SiN_x:H films can be used but relatively thick a-Si:H films should be used in the proposed method.

For PECVD amorphous materials the refractive indices are not always constant, and they vary with deposition conditions. Most reference values of refractive indices are measured in the visible region, which are different from those in the IR region. Therefore, the judgment of right incident angles should be based on whether the baseline of the recorded spectrum is straight and horizontal or not. As a matter of fact, the incident angle at which a straight baseline spectrum is recorded can be used to derive a more accurate value of refractive index in the IR region.

IV. INFLUENCE OF BEAM INCIDENT CONDITION ON SPECTRA

The nuisance of the fringes in terms of distorting the spectra is illustrated by the significant difference between the spectra recorded at various incident conditions in Fig. 3, where spectra variation with the probe beam's polarization state and incident angle is given in Figs. 3(a), 3(b) and 3(c) for a-SiN_x:H, and Figs. 3(d), 3(e) and 3(f) for a-Si:H, respectively. The a-SiN_x:H thin film was about 100 nm thick such that its baseline is straight which can then be leveled easily (film on wedge Si wafer has a similar spectrum); on the other hand, the thickness of a-Si:H film was about 900 nm such that its baseline follows a clear fringe pattern which can then be matched mathematically with less difficulties.

A. a-SiN_x:H thin film

In Fig. 3(a), a p-polarized probe beam strikes the surface of the film at various angles and resulting vibrational absorption spectra have quite different features. The baseline starts from positive slope at a normal incidence to horizontal line (zero slope) at Brewster angle (62° in this case), and then to a negative slope at angles beyond Brewster. The baseline's

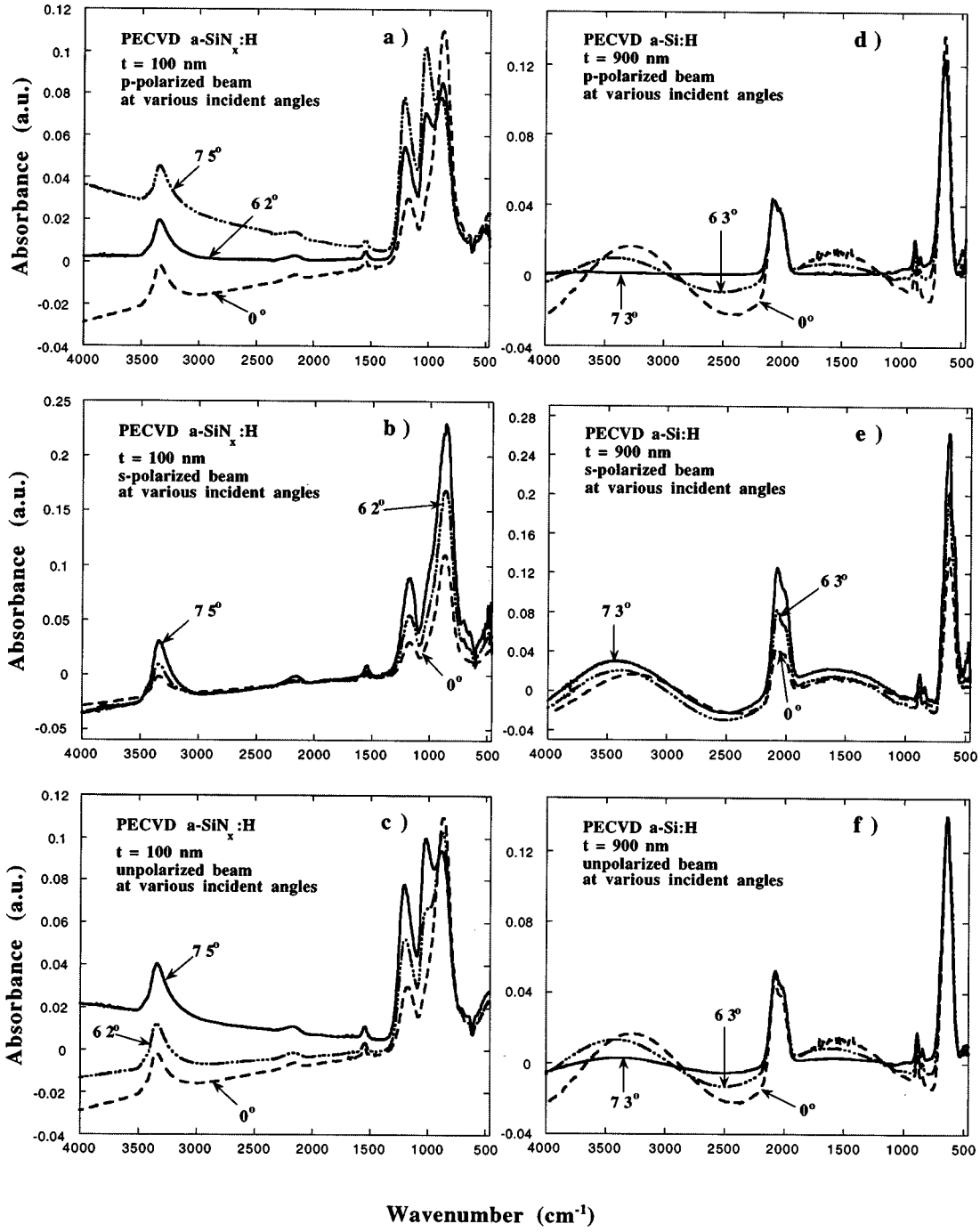

FIG. 3. Influence of probe beam's polarization states and incident angles on vibrational absorption spectra, where (a) and (d) are for *p*-polarized light at various incident angles, (b) and (e) illustrate the situations for *s*-polarized light at various incident angles, (c) and (f) illustrate unpolarized light at various incident angles, for *a*-SiN_x:H and *a*-Si:H thin films, respectively. Brewster angles at *p* polarization are 62° and 73° for *a*-SiN_x:H and *a*-Si:H, respectively.

slope changes clockwise with the increase of incident angle. The change of baseline and peak features follows the pattern of *p*-polarized reflectance in Fig. 2, in which R_p decreases and increases with the increment of incident angle before and after the *B* angle, respectively. In other words, the interference effect on the shape of the spectra is reduced before the *B* angle and then intensified after the *B* angle with the increase of light incident angle.

Figure 3(b) on the other hand illustrates the situation when the *s*-polarized beam passes through the film at various angles. In this case, the baseline is slightly twisted counterclockwise when the incident angle increases. Most prominent of the features in this figure, however, is that the vibrational absorption densities are greatly intensified. This enhancement can be explained again by the *s* curve in Fig. 2, where the increase of reflectance R_s greatly enhances multiple reflection within the film and makes effective thickness of the film much larger than the real value. It should be noted, conceptually, that when the incident angle increases, the film becomes thicker effectively, which also contributes to the increased vibrational absorption density. However, the contribution due to increased thickness is trivial compared to

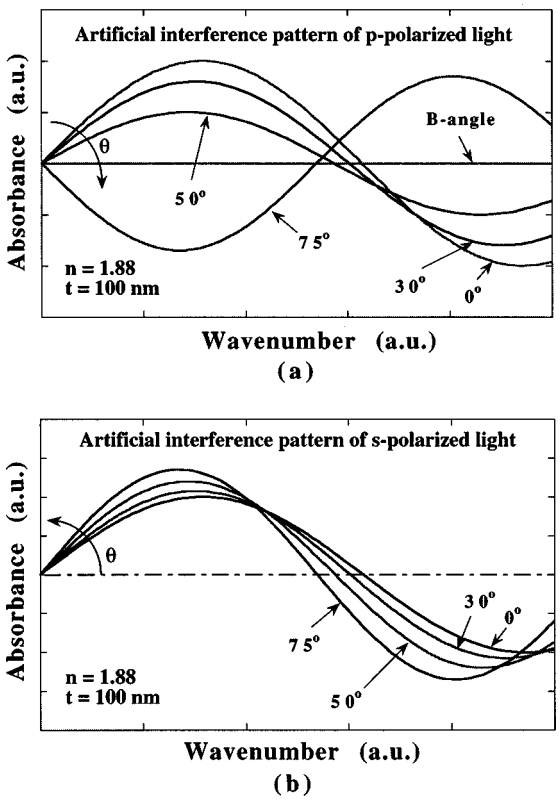

FIG. 4. Interference fringe simulation for: (a) *p*- and (b) *s*-polarized spectra. The refractive index and film thickness used in this simulation are 1.88 and 100 nm, respectively. The angles indicated in the figures are external incident angles.

that caused by multiple reflection, which can be easily verified by thickness normalization. This triviality is also confirmed by the fact that in Fig. 3(a) the overall intensity of the leftmost peak [NH(s) bond] does not change much with various incident angles although the shape varies due to the interference effect, while in Fig. 3(b) the peak intensity changes dramatically with the various incident angles. In the former case, taking 0° and 75°, for example, the spectra's difference is primarily caused by the different effective thicknesses since the reflectances at both angles remain close. By contrast, in the latter, reflectance increases significantly from 0° to 75° (Fig. 2), and plays an important role in peaks reshaping.

It must be noted that the interference pattern alters the spectrum's baseline more seriously in *p*-polarized case than in *s*-polarized spectra, and the rotations of the baseline slopes follow opposite directions with the incident angle in two cases. These observations can well be explained with the help of mathematically generated fringes shown in Fig. 4. The patterns in Figs. 4(a) and 4(b) simulate fringe variations at different incident angles for *p*- and *s*-polarized lights, respectively, and are based on model of interference irradiance distribution[15]

$$I = 4I_0 \cos^2\left(\frac{2\pi n t \omega}{\cos\theta_2}\right), \tag{6}$$

where $4I_0$ is the maximum irradiance which is proportional to the interface reflectance, n is the refractive index of the film, t is the film thickness, ω is the frequency, and θ_2 is the refracted angle and can be derived from $\sin\theta_1 = n \times \sin\theta_2$. For simplicity, n in the simulation is set at a constant of 1.88.

As indicated in Fig. 4(a), for *p*-polarized light, with the increase of the incident angle, the interfacial reflectance and optical path decreases and increases, respectively, and both the fringe amplitude and the spacing are, therefore, decreased. At Brewster angle, the fringe pattern becomes a straight line since interfacial reflectance vanishes at this angle. With the further increase of the incident angle, the amplitude of the fringe increases again with the increasing interfacial reflectance. However, the curvature or phase of the fringe has been changed by 180° [a close observation of baselines in Fig. 3(a) indicates a subtle curvature difference, namely, concave at 75° and convex at 0°, which is consistent with the artificial pattern]. Consequently, a clockwise rotation of the fringe segment at the leftmost part with the increase of incident angle is observed. On the other hand, in Fig. 4(b), for *s*-polarized light, both interfacial reflectance and optical path increase with the incident angle, and thus amplitude and spacing of fringes are increased and decreased with the incident angle, respectively. A counter-clockwise rotation of the fringe segment at the leftmost part with the increase of incident angle is observed correspondingly. Since the baseline of *a*-SiN_x:H spectrum shown in Fig. 3 is only a small segment of the fringes, assuming the leftmost quarter in Fig. 4 for instance, the change of the *p*-polarized baseline is dramatic while the *s*-polarized baseline is moderate or small.

Spectra recorded under unpolarized light beam illumination are presented in Fig. 3(c) for corresponding incident angles again. The curves in this figure resemble *p*-polarized spectra in many aspects and are not the average of *p*- and *s*-polarized curves. This is attributed to a partial polarization of the light when an unpolarized beam incidents at oblique angle. Specifically, with increased incident angle (less than *B* angle), the reflection of *p* and *s* vector at the film's surface is decreased and increased, respectively. Thus, more *p*- and less *s*-polarized light will penetrate into the film as the angle approaches the *B* point. Even when the incident angle is beyond the *B* point, the reflection of *p*-polarized light is still much less than that of *s*-polarized light, although *p*-polarized reflectance also increases with incident angle (Fig. 2). Consequently, light passing through the film at an oblique angle has a partially polarized nature with much more *p*-polarized content than *s*-polarized counterpart, and behaves more like *p*-polarized light.

B. *a*-Si:H thin film

Figures 3(d), 3(e) and 3(f) illustrate the polarization and incident angle influence on *a*-Si:H's vibrational absorption spectra when the film's thickness is increased. The spectra can be explained by the same physics used above for *a*-SiN_x:H, although some specific features are different in these two cases. The fringe pattern clearly follows the model in Fig. 2(b) for *p*-polarized light [Fig. 3(d)], that is, the fringe's amplitude and spacing decrease with a decreasing reflectance (R_{1p}) and increasing incident angle. (Note that

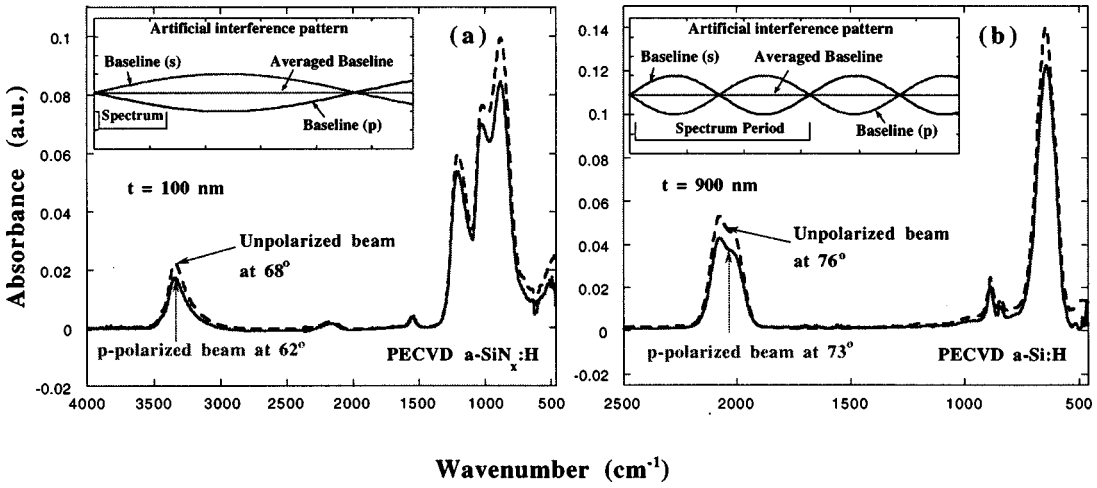

FIG. 5. Comparison between interference fringe-free and virtual fringe-free spectra for (a) a-SiN_x:H and (b) a-Si:H. The insets are mathematically generated fringe patterns simulating the spectra baseline variation. Baseline (p), (s) and averaged baseline represent the baselines of p-, and s-polarized and summation of p- and s-polarized light, respectively. Spectrum period indicates the spectrum range in the simulated fringes.

the spacing or period difference between spectra collected at different angles is very subtle, since the difference between refracted angles and effective thicknesses in those cases is very small due to a large refractive index of a-Si:H thin films.) At B angle (73°), R_{1p} is zero and a straight baseline is observed. When only the s-polarized beam is applied [Fig. 3(e)], fringe amplitude increases and spacing decreases with the incident angle since both the reflectance R_{1s} and the optical path increase with the incident angle. The absorption densities in these s-polarized spectra are increased more significantly than the fringe's amplitude, which is caused by the multiabsorption effect in the film due to the high-reflection nature of s-polarized light. When an unpolarized beam probes the film, the variation of absorption spectra looks like that of p-polarized light due to the same reason stated in the a-SiN_x:H case. Since the splitting of s and p curves is larger in a-Si:H than in a-SiN_x:H films, especially beyond the Brewster angle, the unpolarized beam generated spectra are closer to p-polarized spectra in a-Si:H than in a-SiN_x:H. The baseline variation of a-Si:H spectra under different conditions can also be illustrated conceptually by Fig. 4. The simulation of fringes of a-Si:H (not shown) is, in fact, a modified pattern of Fig. 4, in which a small spacing difference and more than one period spectrum coverage is observed due to the larger values of film thickness and refractive index.

C. Virtual fringe-free spectra

It is not hard to realize that a straight and horizontal baseline can be achieved beyond Brewster angle even with an unpolarized probe beam if we follow the trend in Figs. 3(c) and 3(f). Spectra with such straight and horizontal baselines are recorded at 68° and 76° for a-SiN_x:H and a-Si:H, respectively, and plotted in Figs. 5(a) and 5(b) in comparison to their p-polarized B-angle recorded counterparts. These ''fringe-free'' spectra can be realized because of the counterbalance between the fringe patterns of p- and s-polarized components beyond Brewster angle. As explained previously, the phase change of p-polarized light beyond B angle makes the baseline of spectrum flip from concave to convex, or vice versa, while the curvature of s-polarized light spectra always remain the same although the magnitude increases with the incident angle. Namely, the curvatures of s- and p-polarized components are in opposite direction beyond B angle. An unpolarized light penetrating the film is a partially p-polarized beam, and the spectrum is merely the superimposition of a heavily weighed p-polarized and a lightly weighed s-polarized spectra with opposite curvatures. When the energies of these p- and s-polarized lights in the film reach an equivalency, their fringes balance each other to yield a straight baseline in the spectrum. These conditions for a-SiN_x:H and a-Si:H thin films used in this study are simulated and illustrated in the insets of Figs. 5(a) and 5(b), respectively. Although fringes vanish in such kinds of spectrum, it is still an interference-embedded spectrum, and thus, may be labeled as a ''virtual fringe-free'' spectrum to distinguish it from the ''interference-free'' spectrum. Theoretical determination of light incident angle that results in a virtual fringe-free spectrum is quite complicated and the derivation will be presented elsewhere.[20]

The spectra in Figs. 5(a) and 5(b) illustrate virtual fringe-free spectra of a-SiN_x:H and a-Si:H thin films, respectively. For a-SiN_x:H, 68° is where the s- and p-polarized energies balance each other and yield a straight and horizontal baseline. Likewise, for a-Si:H thin film, 76° is the incident angle at which this counteraction reaches perfection. It is also illustrated in Fig. 5 that virtual fringe-free spectra have larger bond densities than interference-free spectra. In fact, in virtual fringe-free spectra the multireflection still exists and plays a significant role in intensifying the vibrational absorption of bonds although baseline of the spectrum is straight and horizontal. These virtual fringe-free spectra have an undistorted peak feature, and can be used for bonding features (peak shapes) characterization and film microstructure analysis. However, if quantitative analysis is

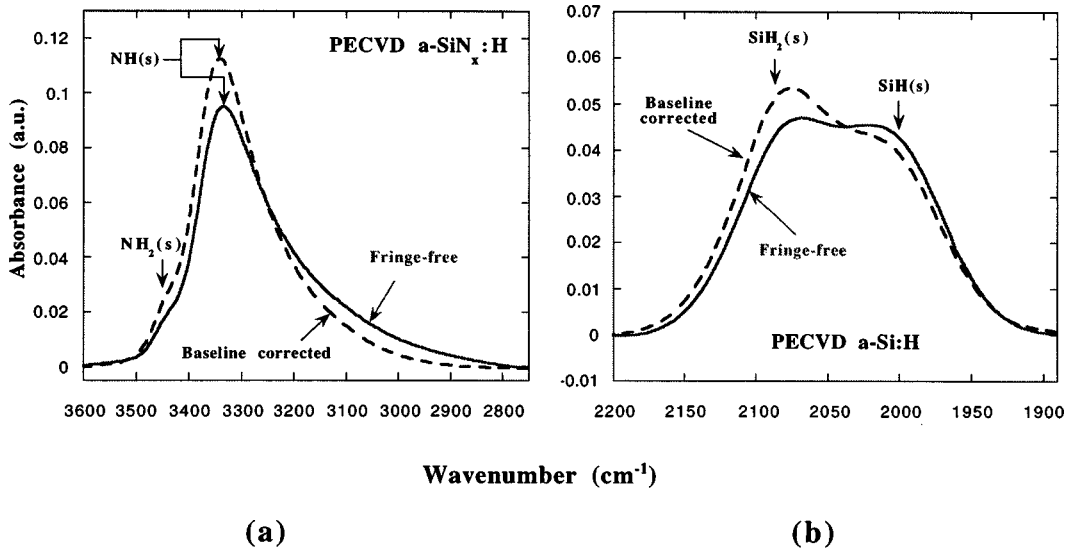

FIG. 6. Comparison between fringe-free spectra and conventionally fringe-corrected spectra for (a) a-SiN_x:H, (b) a-Si:H. Script s in brackets stands for stretching mode vibration.

involved,[13–16] only *B*-angle spectra should be used, since multireflection intensified bond densities will result in an inaccurate assessment of the film microstructure.

It is observed in spectra of a-SiN_x:H that the so-called asymmetrical peak or peaks with a shoulder in the conventional spectra normally contains hidden peaks. These peaks are emerged out or embedded in the cluster according to the incident condition of the probe beam. Therefore, features such as shoulders in the conventional spectra should be especially noted. A detailed discussion about these new features is beyond the scope of this paper and can be found elsewhere.[21]

D. Comparison between fringe-free and conventional spectra

Figure 6 illustrates the flaws of conventional fringe-removal measures, whereas a comparison between ideal (fringe-free) and conventional baseline-corrected spectra is given for (a) a-SiN_x:H between 2750 and 3600 cm^{-1} and, (b) a-Si:H between 1990 and 2200 cm^{-1}, respectively. Conventionally a baseline-corrected spectrum was recorded at normal incidence with the unpolarized beam and then subtracted by using a fringe pattern that matches the spectrum baseline. It is shown in Fig. 6(a) (a-SiN_x:H) that in conventionally baseline-corrected spectrum, with respect to the ideal situation, the peak position of NH(s) is slightly shifted towards a higher wave number and its right shoulder is reduced, while the NH_2(s) density and left shoulder of NH(s) bonds are enlarged. If NH(s) and NH_2(s) bond densities are differentiated out from this peak cluster, the fringe-free and conventionally baseline-corrected spectra will give a different NH_2(s) to NH(s) ratio. Likewise, in Fig. 6(b) (a-Si:H), a nontrivial difference between conventional and ideal spectra is again clearly illustrated, in which the densities ratio of SiH_2(s) to SiH(s) are seriously distorted in conventionally baseline-corrected spectrum. In particular, conventional spectrum has enhanced Si-H_2(s) and reduced Si-H(s) densities in comparison with the fringe-free spectrum. Film's microstructure assessment based on these two spectra will inevitably draw different conclusions for the same film microstructure. Therefore, it is clear that the vibrational absorption spectrum recorded at Brewster angle with *p*-polarized light incidence is the optimal spectrum for hydrogenated amorphous thin-film microstructure characterization.

V. CONCLUSION

We have presented a comprehensive analysis of the probe beam's polarization state and incident angle impact on thin film's vibrational absorption spectra and, hence, proposed a method of scanning thin-film samples in an interference fringe-free environment by utilizing the fact that at Brewster incident angle the *p*-polarized light beam undergoes zero reflection at the interface. Analysis also indicates that a straight-baseline spectra can be realized using the unpolarized beam at a proper incident angle greater than Brewster angle. These kinds of spectra can be used for a qualitative comparison, though they are invalid for a quantitative analysis due to intensified bond densities. Finally, a comparison between conventionally baseline-corrected and ideal spectra unveils a nontrivial feature discrepancy and implies the flaws in the thin-film microstructure analysis reported in the past in the literature.

ACKNOWLEDGMENTS

This work was supported by AFOSR/ARPA through Multidisciplinary University Research Initiative (MURI) under the Contract No. F49020-95-1-0524, and by Center for Display Technology and Manufacturing at the University of Michigan.

[1] N. S. Zhou, S. Fjuita, and A. Sasaki, J. Electron. Mater. **14**, 55 (1985).
[2] J. W. Osenbach, J. L. Zell, W. R. Knolle, and L. J. Howard, J. Appl. Phys. **67**, 6830 (1990).
[3] C. T. Kirk, Phys. Rev. B **38**, 1255 (1988).

[4] S. Hasegawa, L. He, Y. Amano, and T. Inokuma, Phys. Rev. B **48**, 5315 (1993).
[5] N. Maley, A. Myers, M. Pinarbasi, D. Leet, J. R. Abelson, and J. A. Thornton, J. Vac. Sci. Technol. A **7**, 1267 (1989).
[6] N. Maley and I. Szafranek, Mater. Res. Soc. Symp. Proc. **192**, 663 (1990).
[7] A. A. Langford, M. L. Fleet, B. P Nelson, W. A. Lanford, and N. Maley, Phys. Rev. B **45**, 13367 (1992).
[8] I. J. Auer, R. Meisels, and F. Kuchar, Infrared Phys. Technol. **38**, 223 (1997); O. S. Heavens, *Optical Properties of Thin Solid Films* (Butterworths, London, 1955).
[9] B. Reynes, C. Ance, J. P. Stoquert, and J. C. Bruyere, Thin Solid Films **203**, 87 (1991).
[10] T. Li, C. Y. Chen, C. T. Malone, and J. Kanicki, Mater. Res. Soc. Symp. Proc. **424**, 43 (1996).
[11] R. C. Budhani, S. Prakash, H. J. Doerr, and R. F. Bunshah, J. Vac. Sci. Technol. A **5**, 1644 (1987).
[12] H. J. Schliwinski, U. Schnakenberg, W. Windbracke, H. Neff, and P. Lange, J. Electrochem. Soc. **139**, 1730 (1992).
[13] W. A. Lanford and M. J. Rand, J. Appl. Phys. **49**, 2473 (1978).
[14] H. Shanks, C. J. Fang, L. Ley, M. Cardona, F. J. Demond, and S. Kalbitzer, Phys. Status Solidi B **100**, 43 (1980).
[15] A. Morimoto, I. Kobayashi, M. Kumeda, and T. Shimizu, Jpn. J. Appl. Phys., Part 2 **25**, L752 (1986).
[16] E. Bustarret, M. Bensouda, M. C. Habrard, J. C. Bruyere, S. Poulin, and S. C. Gujrathi, Phys. Rev. B **38**, 8171 (1988).
[17] T. Li and J. Kanicki, Phys. Rev. B (submitted).
[18] N. J. Harrick, Appl. Spectrosc. **31**, 548 (1977).
[19] E. Hecht, Optics, 2nd ed. (Addison-Wesley, Reading, MA, 1989), Chap. 8.
[20] T. Li and J. Kanicki (unpublished).
[21] T. Li and J. Kanicki, Mater. Res. Soc. Symp. Proc. (to be published).